

Isotopic fractionation of the major elements of molten basalt by chemical and thermal diffusion

Frank M. Richter^{a,*}, E. Bruce Watson^b, Ruslan Mendybaev^a, Nicolas Dauphas^a, Bastian Georg^c, James Watkins^d, John Valley^e

^a Department of the Geophysical Sciences, The University of Chicago, 5734 South Ellis Avenue, Chicago, IL 60637, USA

^b Department of Earth & Environmental Sciences, Rensselaer Polytechnic Institute, Troy, NY 12180, USA

^c Department of Earth Sciences, Oxford University, Oxford, UK

^d Department of Earth and Planetary Sciences, University of California, Berkeley, CA 94720, USA

^e Department of Geology and Geophysics, University of Wisconsin, Madison, WI 53706, USA

Received 11 November 2008; accepted in revised form 8 April 2009; available online 24 April 2009

Abstract

Samples produced in piston cylinder experiments were used to document the thermal isotopic fractionation of all the major elements of basalt except for aluminum and the fractionation of iron isotopes by chemical diffusion between a natural basalt and rhyolite. The thermal isotopic fractionations are summarized in terms of a parameter Ω_i defined as the fractionation in per mil per 100 °C per atomic mass units difference between the isotopes. For molten basalt we report $\Omega_{Ca} = 1.6$, $\Omega_{Fe} = 1.1$, $\Omega_{Si} = 0.6$, $\Omega_O = 1.5$. In an earlier paper we reported $\Omega_{Mg} = 3.6$. These fractionations represent a steady state balance between thermal diffusion and chemical diffusion with the mass dependence of the thermal diffusion coefficient being significantly larger than the mass dependence of the chemical diffusion coefficients for isotopes of the same element. The iron isotopic measurements of the basalt–rhyolite diffusion couple showed significant fractionation that are parameterized in terms of a parameter $\beta_{Fe} = 0.03$ when the ratio of the diffusion coefficients D_{54} and D_{56} of ^{54}Fe and ^{56}Fe is expressed in terms of the atomic mass as $D_{54}/D_{56} = (56/54)^{\beta_{Fe}}$. This value of β_{Fe} is smaller than what we had measured earlier for lithium, magnesium and calcium (i.e., $\beta_{Li} = 0.215$, $\beta_{Ca} = 0.05$, $\beta_{Mg} = 0.05$) but still significant when one takes into account the high precision with which iron isotopic compositions can be measured (i.e., $\pm 0.03\%$) and that iron isotope fractionations at magmatic temperatures from other causes are extremely small. In a closing section we discuss technological and geological applications of isotopic fractionations driven by either or both chemical and thermal gradients.

© 2009 Elsevier Ltd. All rights reserved.

1. INTRODUCTION

The work reported here expands earlier results that showed large fractionations of lithium and calcium isotopes by chemical diffusion between molten basalt and rhyolite (Richter et al., 2003) and large fractionations of magnesium isotopes in molten silicates by both chemical and thermal diffusion (Richter et al., 2008). We continue to focus on basalt and rhyolite because of their pervasiveness as igneous

rocks and because of their large difference in major element composition, which amplifies the effects we seek to measure. The term chemical diffusion is used here to refer to situations where the flux of chemical components is driven by gradients in composition. The term thermal diffusion, often called Soret diffusion, is used to refer to situations where chemical fluxes are driven by differences in temperature. The ideal experiment for studying isotopic fractionations by chemical diffusion would be one in which two materials of distinct composition are juxtaposed and annealed for a prescribed length of time under isothermal conditions. The duration of such an experiment has to be short compared to time it would take for diffusion to homogenize

* Corresponding author.

E-mail address: richter@geosci.uchicago.edu (F.M. Richter).

the system. The ideal experiment for studying thermal isotope fractionations would be one in which a homogeneous starting material is placed in a temperature gradient and held for a sufficiently long time for the system to reach a steady state.

New isotopic measurements of the run products of a molten basalt thermal diffusion experiment show that all the major elements except monoisotopic aluminum (i.e., calcium, magnesium, iron, silicon, and oxygen) are significantly fractionated by a temperature difference of 100 °C. The piston cylinder sample that was analyzed to determine the thermal isotopic fractionations of calcium, iron, silicon, and oxygen (SRT4) is the same one used by Richter et al. (2008) to measure the thermal fractionation of magnesium isotopes. This allows us to make a direct comparison of the relative thermal fractionations of all the major element isotopic systems of basalt. The thermal isotopic fractionations are summarized by a parameter Ω_i defined as the isotopic fractionation in per mil per 100 °C per atomic mass unit (amu) difference between the isotopes. Richter et al. (2008) reported a value of $\Omega_{\text{Mg}} = 3.6\text{‰}/100\text{ °C amu}$ for the thermal isotopic fractionation of magnesium in molten basalt. Our new results show that the thermal fractionation of the isotopes the other major elements of basalt are all greater than $0.5\text{‰}/100\text{ °C}$ (i.e., $\Omega_{\text{Ca}} = 1.6\text{‰}/100\text{ °C}$, $\Omega_{\text{Fe}} = 1.1\text{‰}/100\text{ °C}$, $\Omega_{\text{O}} = 1.5\text{‰}/100\text{ °C}$, $\Omega_{\text{Si}} = 0.6\text{‰}/100\text{ °C}$, in each case for a difference of one amu).

The rhyolite-basalt piston cylinder diffusion couple that was used to measure iron isotope fractionations by chemical diffusion is the same one that was used by Richter et al. (2008) to determine magnesium isotope fractionations as magnesium diffused from molten basalt into molten rhyolite. The iron isotopic measurements showed that despite our best efforts, the sample was not sufficiently uniform in temperature for the thermal isotopic fractionations to be negligible compared to those due to chemical diffusion. However, having separately determined the effect of a thermal gradient on the isotopic fractionation of iron allowed for a reasonably good estimate of the small but resolvable isotopic fractionation of iron by chemical diffusion.

In the next section, we describe the piston cylinder experiments used to make the diffusion couples and the analytical methods used to measure the isotopic composition of the run products. Subsequent sections discuss the resulting isotopic fractionations in molten basalt by thermal diffusion and the isotopic fractionation of iron by both thermal and chemical diffusion in a rhyolite-basalt diffusion couple. In a final section, we discuss various potential applications of our results to other types of high-pressure high-temperature experiments, to isotope fractionation during diffusion-limited evaporation, and to double-diffusive interfaces that are expected to have been present in the evolution of layered intrusive systems.

2. EXPERIMENTAL AND ANALYTICAL METHODS

The two diffusion couples used here to further explore isotopic fractionations due to thermal and chemical diffusion were made in a piston cylinder apparatus using either only basalt as the starting material (thermal diffusion experiment SRT4) or by juxtaposing natural basalt and natural rhyolite (chemical diffusion experiment RBX). The composition of the starting materials, SUNY MORB for the basalt and Lake County Obsidian for the rhyolite is given in Table 1 of Richter et al. (2003). Fig. 1 shows a schematic diagram of the piston cylinder assembly used for the RBX experiment. The graphite heater for this assembly was intentionally made with variable thickness in an effort to minimize temperature gradients in the vicinity of the sample. Our best estimate of the temperature during the run is also shown in Fig. 1. Fig. 2 shows a backscattered electron image of the glass recovered from this experiment. The SRT4 assembly was similar to that of RBX except that the sample was 10 mm long rather than 5 mm, and the sample was intentionally displaced from the hotspot of a uniform thickness graphite heater assembly to produce a temperature difference across that sample of about 160 °C (see Richter et al., 2008 for further details regarding the SRT4 assembly). Sample SRT4 was run for 100 h and the measured elemental and isotopic profiles were sufficiently similar to those of a 63.8-h run reported by Richter et al.

Table 1

Experimentally determined parameters governing chemical and thermal fractionation of elements and isotopes in molten silicate liquids. Uncertainties in the various parameters, listed as \pm in the last digit, are based on the range of values in model calculations that give results that fit measured data to within their stated errors or their scatter around the model profiles.

Element	σ oxides. (± 0.0001)	Ω ‰/100 °C amu.	$\beta: D_1/D_2 = (m_2/m_1)^\beta$	$\beta_T: D_T^1/D_T^2 = (m_1/m_2)^{\beta_T}$
Mg	0.0015 ^{a,b}	3.6 \pm 0.1 ^{a,b}	0.05 \pm 0.01 ^b	0.65 \pm 0.05 ^{a,b}
Ca	0.0006 ^a	1.6 \pm 0.1 ^a	0.06 \pm 0.02 ^{c,d}	1.15 \pm 0.05 ^a
Fe	0.0018 ^a	1.1 \pm 0.1 ^a	0.03 \pm 0.01 ^a	0.40 \pm 0.02 ^a
Si	-0.0015 ^a	0.6 \pm 0.2 ^a	—	0.24 \pm 0.0 m1 ^a
Al	~0	—	—	—
O	—	1.5 \pm 0.2 ^a	—	—
Li	—	—	0.215 \pm 0.005 ^c	—
Ge	—	—	<0.025 ^d	—

^a This work.

^b Richter et al. (2008).

^c Richter et al. (2003).

^d Richter et al. (1999).

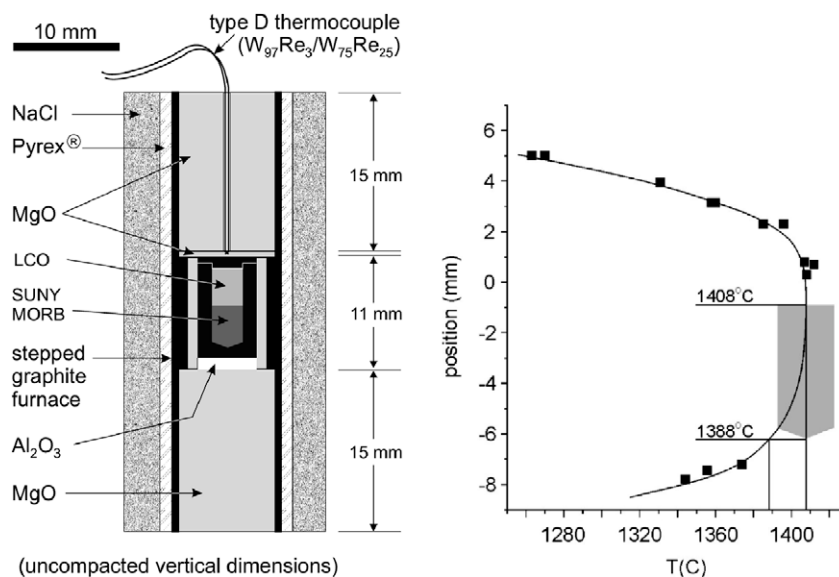


Fig. 1. The diagram on the left shows the piston cylinder assembly used to make sample RBX. The sample was run for 15 h at 1.2 GPa and a nominal temperature of 1400 °C. The graphite heater was made with variable thickness in order to change the local heating rate in an effort to minimize temperature gradients in the sample. The estimated temperature profile during the run is shown on the right. The filled squares show places where temperatures were determined from the thickness of the spinel layer that developed where MgO was in contact with Al₂O₃.

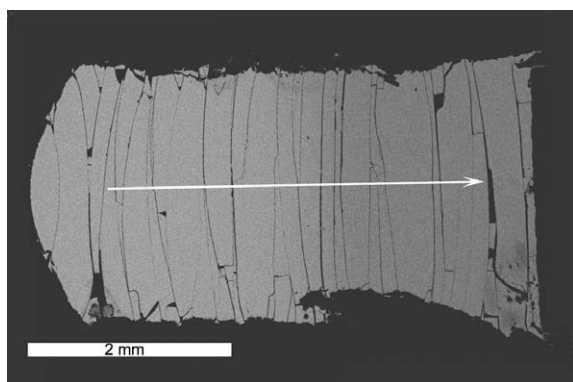


Fig. 2. Backscattered electron image of exposed glass from sample RBX. The arrow is in the direction from basalt to rhyolite and shows the line along which the concentration of the major oxide components was measured. The variation in the gray scale of the backscattered image reflects the gradient in atomic weight.

(2008) that SRT4 can be considered to have effectively reached a steady state. Both RBX and SRT4 were run at pressures slightly in excess of 1 GPa in order that any volatiles that might have remained in the sample after pressurization would dissolve in the melt thus avoiding bubbles that would distort the diffusion profiles as they moved through the sample.

Accurate determinations of isotope fractionations by thermal diffusion require not only high-precision isotopic measurements but also realistic estimates of the temperature distribution in the piston cylinder assembly during run conditions. The temperatures we report are based on the method of Watson et al. (2002) where the progress of the spinel-forming reaction $\text{MgO} + \text{Al}_2\text{O}_3 \rightarrow \text{MgAl}_2\text{O}_4$ is

used to monitor the local temperature. Watson et al. (2002) calibrated the rate at which spinel is formed as a function of both pressure and temperature. Given this calibration and duration of an experiment, the local thickness of the spinel layer that forms wherever MgO and Al₂O₃ were in contact can be used to determine the local temperature. The accuracy of such temperature measurements is about ± 10 °C when compared to thermocouple readings, but better than this in terms of the relative temperature differences between a set of points in the same experiment. Fig. 1 shows the temperatures measured by the spinel reaction thermometer above and below experiment RBX. Fig. 3 shows the spinel-reaction temperature estimates for experiment SRT4. The temperature profiles are interpolated into the molten sample based on temperatures measured by Watson et al. (2002) for the same piston cylinder assembly with MgO and Al₂O₃ juxtaposed at points along the entire assembly.

The recovered piston cylinder samples SRT4 and RBX were polished to expose the quenched glass allowing the major element concentrations to be measured using a JEOL JSM-5800LV scanning electron microscope equipped with an Oxford Link ISIS-300 energy dispersive X-ray microanalysis system. The measured concentration of each spot analyzed is based on rastering a 15 kV primary beam current of 8 nA over a 10 μm square area. At least two profiles were measured for each couple giving an estimated precision of better than 1% relative for the concentrations.

After the major element profiles had been measured, the samples were sectioned perpendicular to their long axis to make a series of approximately 500 μm thick slabs. Selected slabs were dissolved overnight in a 70 °C 3:1 mixture of HF:HNO₃ and then converted to nitric acid solutions by evaporating and redissolving them two or more times in high-purity, double distilled concentrated nitric acid. The

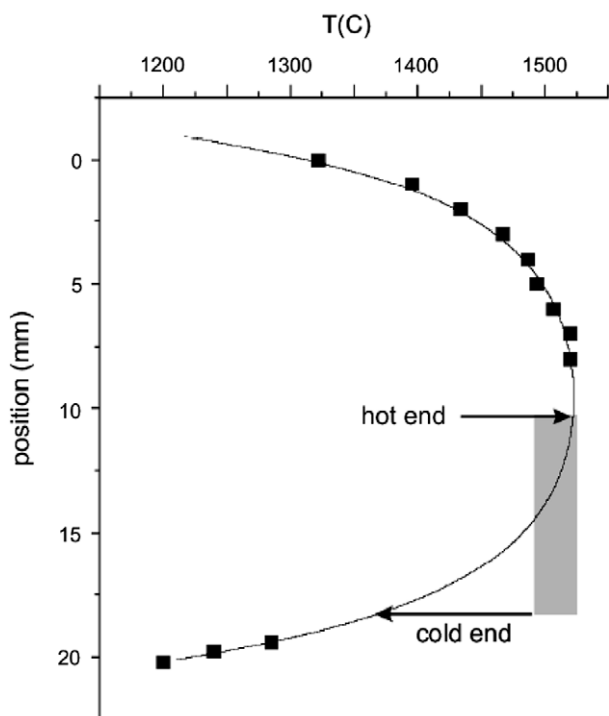


Fig. 3. Temperature distribution in sample SRT4 during the thermal diffusion experiment as determined by the thickness of the spinel layer measured at the places indicated by solid squares. The starting material was homogeneous SUNY MORB basalt. The experiment was run at 1.7 GPa for 100 h with the sample intentionally displaced from the hotspot of the heater assembly in order to impose a temperature difference of about 160 °C from one end to the other.

final redissolution was in 1 N nitric acid. Splits of the dissolved solutions from SRT4 were distributed for separate ion exchange purification of magnesium, calcium, and iron prior to isotopic analysis. A small number of chips of the original glass from SRT4 were sent to the University of Wisconsin for oxygen isotopic analysis and to Oxford University for silicon isotopic analysis. A portion of the dissolved RBX solutions that had been used earlier for the magnesium isotopic measurements reported by Richter et al. (2008) were purified to make an iron solution for isotopic analysis.

2.1. Iron isotopic measurements

Dauphas et al. (2004, in press) described the protocols used for chemical separation and isotopic analysis of iron, and the reader is referred to those papers for the details. The iron solutions were purified using disposable Bio-Rad Poly-Prep columns filled with 1 mL of AGI-X8 200-400 mesh chloride resin previously cleaned and conditioned. Sample solutions were loaded in ~0.2 mL of 6 M HCl, such that the resin/solution partition coefficient of Fe is greater than a factor of 1000 in favor of the resin. Matrix elements other than Fe were eluted in 8 mL of 6 M HCl added to the column in increments of 0.5, 0.5, 1, 2, and 4 mL. Iron was then eluted in 9 mL of 0.4 M HCl added in increments of 0.5, 0.5, 1, 3, and 4 mL. Dauphas et al. (2004, in press)

showed that the yield is 100% and that there is no measurable isotopic fractionation during chemical separation of iron using this anion-exchange column.

The iron isotope measurements were done at the Origins Laboratory at the University of Chicago using a Thermo Scientific Neptune High Resolution MC-ICPMS, and are reported as $\delta^{56}\text{Fe} = \left[\frac{(^{56}\text{Fe}/^{54}\text{Fe})_{\text{sample}}}{(^{56}\text{Fe}/^{54}\text{Fe})_{\text{IRMM-014}}} - 1 \right] \times 1000$ with IRMM-014, which has an isotopic composition very close to chondritic (Dauphas and Rouxel, 2006), used as the reference material. The measurements were performed at a mass resolution that reduced the interferences from ArN^+ , ArO^+ , and ArOH^+ on Fe^+ . Even so, the argide peaks could not be completely resolved from iron and thus the measurements were made on flat-topped peak shoulders. The solutions were introduced into the mass spectrometer using a dual cyclonic-Scott spray chamber (Stable Sample Introduction system). The chemical diffusion experiment involved natural basalt and rhyolite. Measurement of the bulk rhyolite showed elevated $\delta^{56}\text{Fe}$ (0.265‰) relative to the bulk basalt (0.107‰), which had to be taken into account during modeling of the isotope diffusion profile. Accurate $\delta^{56}\text{Fe}$ measurements can be routinely achieved within the quoted uncertainties of around $\pm 0.03\%$ at the 95% confidence level (Dauphas et al., in press).

2.2. Calcium isotopic measurements

Dissolved sample solutions were dried and then redissolved in 1 N nitric acid. An appropriate amount of ^{42}Ca - and ^{48}Ca -enriched double spike was added to each sample to correct for mass discriminations produced by the mass spectrometer itself (see DePaolo, 2004). The dissolved sample-spike mixtures are loaded onto cation exchange columns and eluted with 1.0 N and 1.5 N nitric acid in order to separate Ca from other major cations. About 3 μg of purified Ca from each sample are loaded onto a Re filament and introduced into the mass spectrometer by thermal ionization. The Ca isotope ratio measurements were carried out at the University of California, Berkeley on a Thermo-Finnigan Triton TI with nine moveable Faraday collectors. For each sample, 200 isotope ratio measurements are made in order to reduce uncertainties to about $\pm 0.15\%$. The measured ratios from the mass spectrometer are for the spike-sample mixture. The actual sample isotope ratios are determined using an iterative spike-subtraction algorithm summarized in DePaolo (2004) and shown explicitly for Fe isotopes (analogous to Ca isotopes) in Fantle (2005).

Ca isotope ratios are reported as $\delta^{44}\text{Ca} = \left[\frac{(^{44}\text{Ca}/^{40}\text{Ca})_{\text{sample}}}{(^{44}\text{Ca}/^{40}\text{Ca})_{\text{std}}} - 1 \right] \times 1000$, where the standard is an ultra-pure CaCO_3 with $(^{44}\text{Ca}/^{40}\text{Ca})_{\text{std}} = 0.0212076$ (Skulan et al., 1997). On this scale, the average value of terrestrial igneous rocks is $\delta^{44}\text{Ca} \sim 0\%$ and the total range is -0.33% to $+0.37\%$ (as quoted in Richter et al., 2003).

2.3. Silicon isotopic measurements

Glass chips from STR4 (~1 mg each) were fused for 10 min at 720 °C in Ag crucibles, with solid NaOH as the

flux medium. Fusion cakes were subsequently dissolved in 20 ml deionized water (MilliQ-element, MilliPore) and finally transferred into 1% HNO₃ solutions. The silicate cationic matrix and the flux matrix were removed by cation exchange chromatography on Bio-Rad columns packed with 1.9 ml of AG 50 W-X12 (200–400 mesh) cation exchange resin. A detailed description of the entire procedure is given in [Georg et al. \(2006\)](#). The one difference from the published procedures is that all samples were acidified with HNO₃, instead of HCl. All Si isotope standards, NBS-28, IRMM-018, Diatomite, and BigBatch were prepared in a similar manner to ensure acid matrix match between sample and standard solutions. In addition to these standards, three independent batches of the USGS rock standard BHVO-1 were prepared, to ensure the absence of matrix effects for basaltic rock matrices.

The isotopic composition was analysed using a NuPlasma HR high-resolution multiple collector inductively coupled plasma mass-spectrometer (HR-MC-ICP-MS) at the Department of Earth Sciences in Oxford. The instrumental mass bias was corrected by a standard-sample bracketing protocol. Samples were taken up via a self-aspirating 6 mm concentric micro-flow PFA nebuliser with typical uptake rates around 80 $\mu\text{l min}^{-1}$ and aspirated into a DSN-100 (Nu Instruments) desolvation device. The dry sample aerosol is introduced into the plasma using a semidismountable torch equipped with a sapphire injector (Elemental Scientific Inc.). Each sample was analysed at least 11 times where each analysis represents one sample run and two bracketed standard runs. The silicon isotope data are reported as deviations of ³⁰Si/²⁸Si from the international standard NBS-28 in the standard notation $\delta^{30}\text{Si} = \left[\frac{(^{30}\text{Si}/^{28}\text{Si})_{\text{sample}}}{(^{30}\text{Si}/^{28}\text{Si})_{\text{NBS28}}} - 1 \right] \times 1000$.

2.4. Oxygen isotopic measurements

Oxygen isotope ratios of 0.5–2 mg pieces of glass were analyzed at the University of Wisconsin–Madison by laser fluorination. Oxygen was liberated by reaction with BrF₅, reacted with hot graphite, and converted into CO₂, following the procedures described by [Valley et al. \(1995\)](#). Values of $\delta^{18}\text{O}$ were determined in a Finnigan MAT 251 mass-spectrometer. A total of 11 aliquots of UWG-2 garnet standard were analyzed before and after the samples with a precision of $\pm 0.09\text{‰}$ (1 sd). The raw value for UWG-2 differed by 0.27‰ from the accepted value of 5.80‰ on the Vienna Standard Mean Ocean Water (VSMOW) scale, and analyses of samples have been corrected, as described in [Valley et al. \(1995\)](#). All results are reported in the standard notation $\delta^{18}\text{O} = \left[\frac{(^{18}\text{O}/^{16}\text{O})_{\text{sample}}}{(^{18}\text{O}/^{16}\text{O})_{\text{VSMOW}}} - 1 \right] \times 1000$.

3. ISOTOPE FRACTIONATION BY THERMAL DIFFUSION

[Fig. 4](#) shows the measured mole fractions of the major oxide components in the basalt sample SRT4 that was run in a piston cylinder for 100 h at a pressure of 1.7 GPa and temperature ranging from 1360 to 1520 °C. The temperature gradient and associated density differences are in the direction of stabilizing the molten sample against convective overturning. The oxide concentrations measured as a function of position in the sample are plotted as a function of temperature using the temperature distribution shown in [Fig. 3](#). The chemical gradients that developed in response to the difference in temperature along the long axis of the sample are typical of thermal fractionations in silicate liquids (see, for example, [Leshner and Walker, 1986](#))

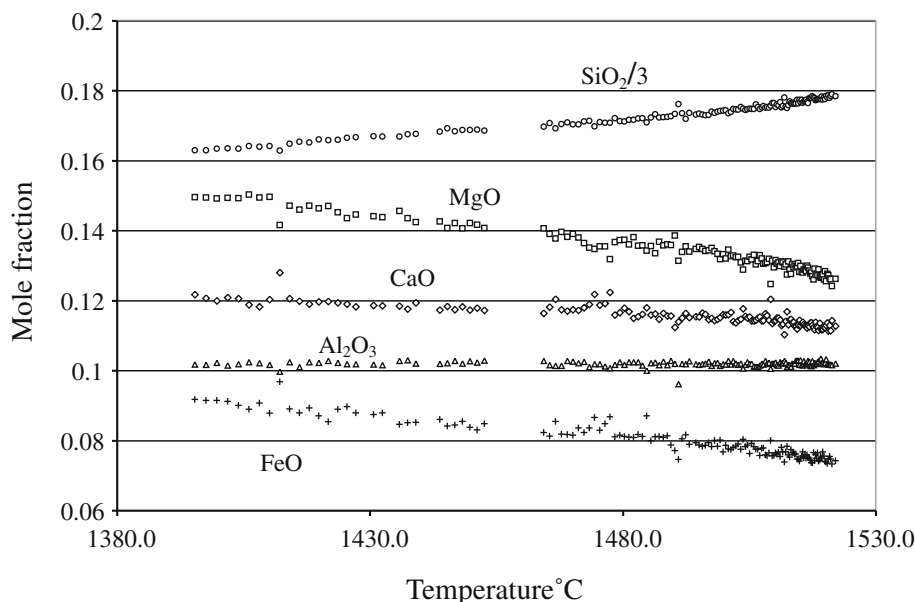


[Fig. 4](#). Concentration of the major oxides measured along the long axis of sample SRT4 plotted as mole fractions versus temperature using the temperature distribution shown in [Fig. 3](#). Note that for silica the values are 1/3 the mole fraction of SiO₂. The data gap at temperatures around 1460 °C is due to part of the sample being lost due to plucking during polishing.

with the MgO, CaO, FeO components increasing towards the cold end, SiO₂ enriched at the hot end, and much smaller change in the Al₂O₃ component.

The main focus of the work reported here was to document the isotopic fractionations of the major elements of basalt that arise as a result of a temperature difference maintained across molten basalt. Richter et al. (2008) have already shown that a temperature change of about 100 °C produced a remarkably large fractionation of ²⁶Mg/²⁴Mg of more than 8‰ with the heavier isotope being enriched at the cold end of the sample. We are now able to show that similar isotopic fractionations occur for calcium, iron, silicon and oxygen. Fig. 5 shows the isotopic composition of calcium and iron as a function of temperature along the axis of sample SRT4 together with the earlier result (Richter et al., 2008) for the thermal fractionation of magnesium isotopes.

The calcium and iron isotopes were measured on splits of the same dissolved sample solutions as used for the magnesium isotope measurements, which allows for a direct comparison of the thermal fractionations of these three isotopic systems. Fig. 6 is a plot of the calcium and iron isotopic fractionations versus that of magnesium. The fact that the calcium and iron fractionations are, within the stated errors, linearly correlated with that of magnesium is good evidence of the consistency of our isotopic measurements and that the reported uncertainties are realistic.

Fig. 7 is the equivalent of Fig. 5 but for the fractionation of oxygen and silicon isotopes as a function of temperature. Note that the increments on the vertical scale of Fig. 7 are half those used in Fig. 5. We cannot make the equivalent of Fig. 6 for oxygen and silicon isotopes versus magnesium isotopes because they were not measured on the same pieces of glass from SRT4. The overall conclusion is that the isotopic fractionations of the major elements of basalt by ther-

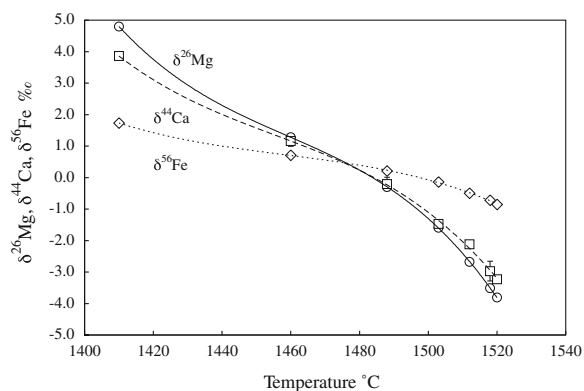


Fig. 5. Isotopic fractionation of ²⁶Mg/²⁴Mg (circles), ⁴⁴Ca/⁴⁰Ca (squares), and ⁵⁶Fe/⁵⁴Fe (diamonds) versus the average temperature of 500 μm slabs cut perpendicular to the long axis of sample SRT4. With two exceptions, the 2σ error bars of the isotopic data are smaller than the symbols used to display the data. The curves through the data are third order polynomial fits that have no theoretical basis and are included simply to guide the eye. The fractionations are reported in delta notation $\delta^iX = 1000 \left(\frac{(^iX/^iX)_{\text{sample}}}{(^iX/^iX)_{\text{SUNY MORB}}} - 1 \right)$ relative to the isotopic composition of the starting SUNY MORB basalt.

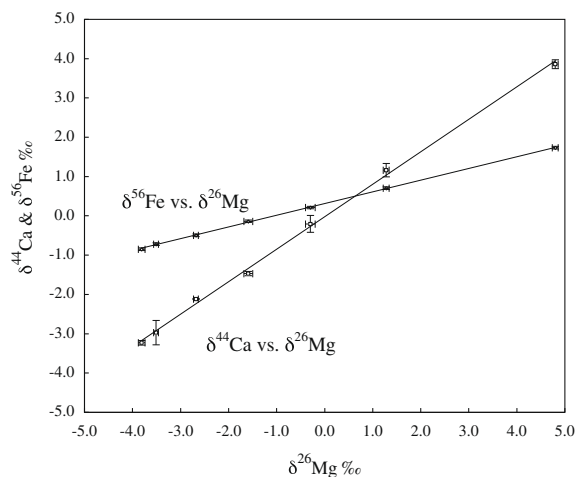


Fig. 6. Same isotopic data as in Fig. 5 but now displayed as the iron and calcium isotopic fractionations versus those of magnesium from the same dissolved samples from SRT4. The lines are least squares linear fits to the data points that are shown with 2σ error bars.

mal gradients (except for aluminum) are highly correlated but with a range of sensitivities to temperature. A good measure of this sensitivity to temperature is given by a parameter Ω , which we define as the fractionation in per mil per 100 °C per atomic mass unit difference between the isotopes. Table 1 lists the values of Ω for magnesium, calcium, iron, silicon, and oxygen that have been measured in molten SUNY MORB basalt. The thermal fractionation parameter for oxygen isotopes reported here is similar to that one derives from the thermal fractionation of oxygen in molten silicate systems reported by Kyser et al. (1998).

Model calculations were used to determine the mass dependence of the parameters governing the elemental and isotopic fractionation associated with temperature differences in molten basalt. The calculations are based on a one-dimensional conservation equation

$$\frac{\partial \rho_i}{\partial t} = -\frac{\partial J_i}{\partial z} \quad (1)$$

where ρ_i is the molar density of element or isotope i (mol/cm³) and J_i is the flux (mol/cm²/s). A pseudo-binary form suggested by Tyrell (1961) was used for the flux (see also deGroot and Mazur, 1984, CH. XI §7)

$$J_i = -D_i \rho \left(\frac{\partial w_i}{\partial z} + \sigma_i w_i w_j \frac{\partial T}{\partial z} \right) \quad (2)$$

where D_i is an effective binary diffusion coefficient of component i in the mixture j , ρ is the molar density of the mixture, w_i and w_j are the mole fractions of i and j , and σ_i is the Soret coefficient. An alternative way of specifying the flux that makes clearer the separate role of chemical diffusion (as determined by D_i and concentration gradients) and thermal diffusion is to define a thermal diffusion coefficient $D_T^i \equiv D_i \sigma_i$ such that

$$J_i = -\rho \left(D_i \frac{\partial w_i}{\partial z} + D_T^i w_i (1 - w_i) \frac{\partial T}{\partial z} \right) \quad (3)$$

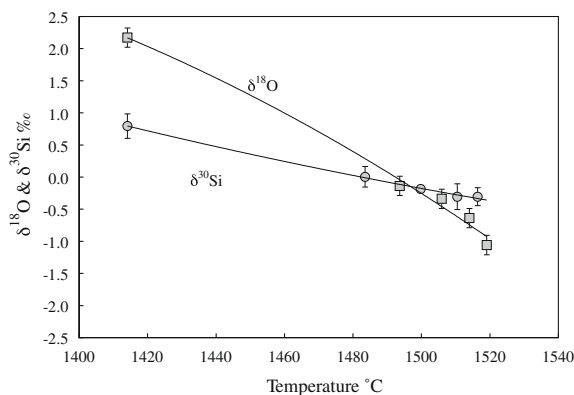


Fig. 7. Same as Fig. 5 but now showing the fractionation of $^{18}\text{O}/^{16}\text{O}$ (squares) and $^{30}\text{Si}/^{28}\text{Si}$ (circles) as a function of temperature. The lines are second order polynomial fits to the data points plotted with 2σ error bars. The polynomial fits have no theoretical basis and are used simply to guide the eye.

When Eq. (3) is used to model the oxide profiles of sample SRT4, and especially RBX, one has to take into account that the effective binary diffusion coefficients depend on the silica content of the melt. For this a parameterization of the form $D_{i(\text{SiO}_2)} = D_{i,o} e^{-\alpha(F_{\text{SiO}_2} - 0.5)}$ is used where F_{SiO_2} is the mole fraction of SiO_2 and α is a parameter to be adjusted by fitting the diffusion profiles. Eqs. (1) and (3) together with this formulation for the effective binary diffusion coefficients result in a conservation equation of the form

$$\frac{\partial w_i}{\partial t} = \frac{\partial}{\partial z} \left[D_{i(\text{SiO}_2)} \frac{\partial w_i}{\partial z} + D_T^i w_i (1 - w_e) \frac{\partial T}{\partial z} \right] \quad (4)$$

The quantity w_e in the last term in brackets is the total mass fraction of the oxide with isotopes represented by i . This use of w_e insures that when Eq. (4) is summed over all the isotopes of an element (i.e., $w_e = \sum w_i$) it becomes the conservation equation for the total element. In writing Eq. (4) we have made the simplification that the total molar density ρ is sufficiently uniform that its derivatives can be neglected compared to the derivatives of the mole fractions and of the temperature. This simplification is justified in that changes in the total molar density due to composition differences are small because the effect of increasing (decreasing) SiO_2 content is for the most part balanced by decreases (increases) in the amount of the other major oxides. The ratio of changes in the total molar volume to that of temperature will be of the order of the thermal expansion coefficient, which is a very small quantity compared to unity. When Eq. (4) is used to model isotope fractionations one has to allow for the possibility that both the chemical and thermal diffusion coefficients are mass dependent, which we parameterized as $D_i/D_j = (m_j/m_i)^\beta$ and $D_T^i/D_T^j = (m_i/m_j)^{\beta_T}$ where m_i and m_j are the atomic mass of isotopes i and j . Note that in contrast to the mass dependence of the chemical diffusion coefficients, for positive β_T the thermal diffusion coefficient will be larger for the heavier isotope.

Richter et al. (2008) showed that the quantity $\beta + \beta_T$ can be determined directly from the steady state change in the

isotopic composition between the hot and cold ends of a thermal diffusion couple (see Eq. (15) in Richter et al., 2008). In the present study we numerically integrated Eq. (4) to steady state with independently measured values for β and various choices of σ and β_T until a satisfactory fit to the data from SRT4 was achieved. We did this to validate the numerical calculations in the steady state limit and thereby give some basis for confidence in our use, below, of the numerical calculations for transient situations. The results also validate the claim that sample SRT4 had reached a steady state.

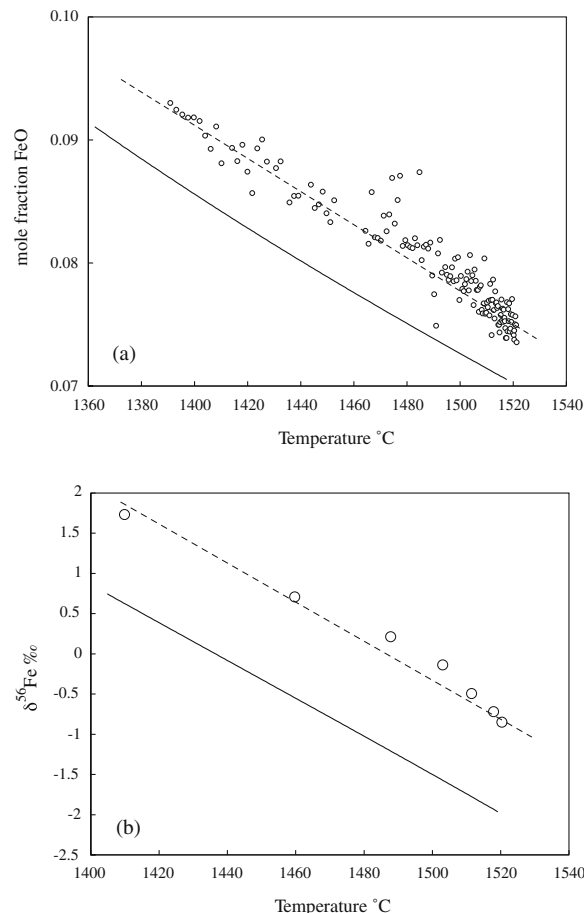


Fig. 8. Model calculations of the thermal effect on the concentration and isotopic composition of iron in molten basalt are compared to data from sample STR4. The model was run for a sufficient length of time for the result to be effectively at steady state. (a) Circles show the measured mole fraction of iron as a function of temperature (same data as in Fig. 4). The solid line shows the result of a model calculation with the same bulk iron concentration as SRT4, a linear temperature gradient, and $\sigma_{\text{Fe}} = D_T^{\text{Fe}^c}/D_{\text{FeO}} = 0.0018$. A dashed line with the same slope as the calculated values has been drawn through the data to show that the calculation reproduces the change in moles of iron versus temperature. (b) Same as (a) but for iron isotope fractionation (same data as in Fig. 5). $\beta = 0.03$ and $\beta_T = 0.40$ were used to fit the isotopic fractionation of iron. The offset between the solid and dashed lines is due to the calculation assuming a uniform temperature gradient while the temperature gradient in SRT4 is steeper at the cold end of the diffusion couple (see text for a discussion of the offset).

Fig. 8 compares a model calculation using Eq. (4) for the changes in the concentration and isotopic fractionation of iron as a function of temperature to the measured data from SRT4. A linear temperature profile was assumed in the calculation. The initial condition was uniform in both concentration and isotopic composition, and a no-flux boundary condition was imposed at each end. Assuming a uniform temperature gradient in the calculation is useful for showing conservation of species in that the midpoint of the concentration and isotopic fractionation profiles should remain at their initial values. For any other temperature profile the steady state concentration and isotopic gradient will be the same as for a linear temperature gradient but displaced by an amount related to the difference between the total temperature change ΔT across the diffusion couple of length L and the integral $\int_{x=0}^{x=L} (dT/dx)dx$. This effect of a nonuniform temperature gradient explains why the measured concentration and isotopic data plotted as a function of temperature appear displaced to positive values relative to the initial composition of the basalt.

Similar calculations to those shown in Fig. 8 were used to match the concentration and isotopic fractionation of magnesium, calcium, and silicon as a function of temperature in sample SRT4. Fitting the gradient of concentration versus temperature provides the estimate of the Soret coefficient, σ_i , for each element. Matching the gradient of isotopic fractionation versus temperature gives an estimate of $\beta + \beta_T$. The values of σ_i and β_T that yield the best least squares linear fit to the concentration and isotopic fractionation data from sample SRT4 are given in Table 1. The values listed in Table 1 for the exponent β that parameterizes the mass dependence of the chemical diffusion coefficients was determined by separate experiments involving chemical diffusion between basalt and rhyolite.

4. IRON ISOTOPE FRACTIONATION BY CHEMICAL DIFFUSION

Iron isotopic measurements of six 500 μm thick slabs from Sample RBX were used to determine the mass dependence of the chemical diffusion coefficient of the iron isotopes in much the same way as was done earlier (Richter et al., 2003, 2008) for calcium, lithium, and magnesium. Model calculations were used to determine the small differences in the diffusion coefficients of the isotopes of a given element. To do this one has to first model the evolution of the parent element. Fig. 9 shows measured mole fractions of FeO and SiO₂ as a function of distance along the long axis of the rhyolite-basalt diffusion couple RBX. The asymmetry of the concentration profiles reflect the fact that the diffusivities of FeO and SiO₂ depend on SiO₂ content of the melt, being significantly larger in the basalt than in the rhyolite. The results of model calculations using Eq. (4) with initial conditions reflecting the mole fractions of FeO and SiO₂ in the basalt and in the rhyolite, and no-flux boundary conditions at each end of the diffusion couple are shown by the solid curves in Fig. 9.

Our main interest in reanalyzing the RBX diffusion couple was to use the measured iron isotopic fractionations to determine the relative mobility of the iron isotopes as they

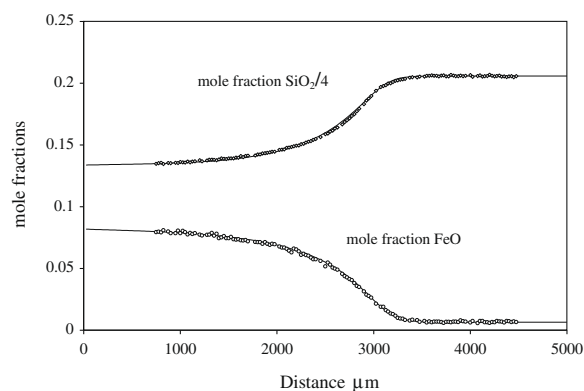


Fig. 9. Mole fractions of SiO₂/4 and FeO measured along the centerline of sample RBX are shown as small open circles. The solid curves were calculated using Eq. (4) with $D_{\text{FeO}} = 1.4D_{\text{SiO}_2}$ for time equal to 0.07 in units of $L^2/4D_{\text{SiO}_2}$ where L is the length of the diffusion couple in centimeters. The variation of the diffusion coefficients D_{FeO} and D_{SiO_2} with the silica content of the melt is parameterized as $e^{-\alpha(F_{\text{SiO}_2}-0.5)}$ where F_{SiO_2} is the mole fraction of SiO₂ and $\alpha = 8.0$ for SiO₂ and 8.5 for FeO.

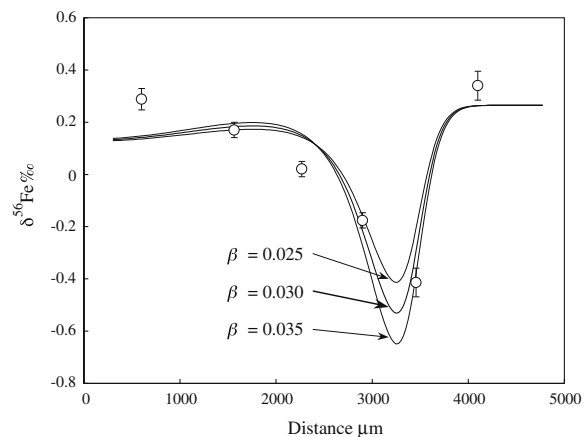


Fig. 10. The open circles show the iron isotopic fractionation relative to the IRMM-014 standard of six 500 μm slabs from RBX plotted at the distance of their center from the basalt end of the diffusion couple. Relative to this standard the isotopic composition of the basalt corresponds to $\delta^{56}\text{Fe} = 0.107 \pm 0.014$ and for the rhyolite, $\delta^{56}\text{Fe} = 0.265 \pm 0.014$. The curves are model results for the average isotopic composition of 500 μm thick slabs calculated using Eq. (4) for ^{56}FeO and ^{54}FeO in the same way as was done for the mole fraction of total FeO shown in Fig. 9. The slightly different isotopic composition of the basalt and the rhyolite used to make the diffusion couple was taken into account in the calculations by the initial conditions. Three choices of β in $D_{^{56}\text{FeO}}/D_{^{54}\text{FeO}} = (54/56)^\beta$ were used to illustrate the sensitivity of the chemical isotope fractionations to this parameter. The temperature was assumed to be uniform in this calculation and thus no thermal isotope fractionation is involved.

diffused from the basalt to the rhyolite. Fig. 10 shows the iron isotopic composition of six 500 μm slabs from RBX plotted at a distance corresponding to their center. The negative $\delta^{56}\text{Fe}$ values in the portion of the sample where iron has diffused from the basalt into the rhyolite is clear

evidence that the chemical diffusion of ^{54}Fe is somewhat faster than that of ^{56}Fe . Fig. 10 shows the iron isotopic data along with three curves calculated using $\beta = 0.025$, 0.030, and 0.035 where β is the exponent in $D_{^{56}\text{FeO}}/D_{^{54}\text{FeO}} = (54/56)^\beta$. These calculations assumed that the temperature was uniform (i.e., no thermal isotope fractionation) and serve to show that the data in the rhyolite half of the couple are reasonably fit by $\beta = 0.030 \pm 0.005$. There is, however, an obvious misfit to the isotopic data in the basalt. The more or less linear decline of the $^{56}\text{Fe}/^{54}\text{Fe}$ data points in the basalt side of the diffusion couple suggest that thermal isotope fractionation was not negligible.

The model calculations shown in Fig. 10 show small gradients in the basalt that are opposite the much larger gradient defined by the data points. The likely cause of this misfit is isotopic fractionations due to the small temperature change shown in Fig. 1. Fig. 11 shows the same calculation as the $\beta = 0.030$ case in Fig. 10 but now for the three choices of the temperature distribution shown in Fig. 12, and with $\sigma_{\text{Fe}} = 0.018$ and $\beta_T = 0.4$. These values of σ_{Fe} and β_T are those that were determined from the analyses of thermal diffusion sample SRT4.

The temperature distribution that results in calculated isotopic fractionations closest to the actual data is case 3 with a total temperature change of 30 °C, which is somewhat larger than was measured by the spinel thermometry (i.e., $\Delta T \sim 20$ °C). For calculations with temperatures corresponding to curves 1 and 2, part of the reason for the misfit is that the fractionations due the temperature changes propagate in from the boundaries and the duration of the high temperature event is sufficiently short that the calculated effect is noticeably greatest near the left hand side boundary. The discontinuity in the temperature gradient in case 3 results in the thermal fractionations propagating from both ends of the gradient region with the result that the entire basalt side of the couple is affected. The difference between the calculated curves and the last data point on the right cannot be reconciled by imposing any reasonable temperature gradient in the rhyolite portion of the couple be-

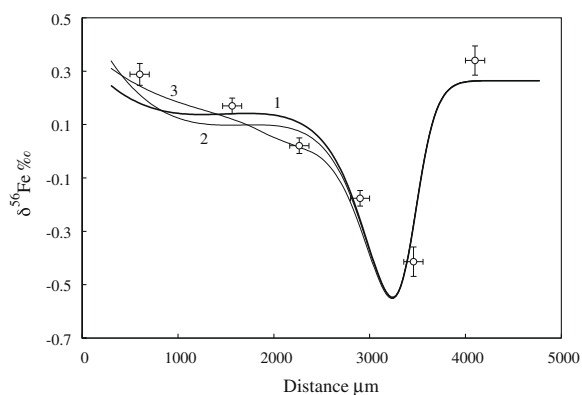


Fig. 11. Model calculations for the combined thermal and chemical isotopic fractionation of iron for the three temperature distributions shown in Fig. 12 and $\beta = 0.030$, $\sigma_{\text{Fe}} = 0.018$, and $\beta_T = 0.40$. The heavier line shows the result when our best estimate of the temperature distribution (as shown in Fig. 1) is used in the calculation.

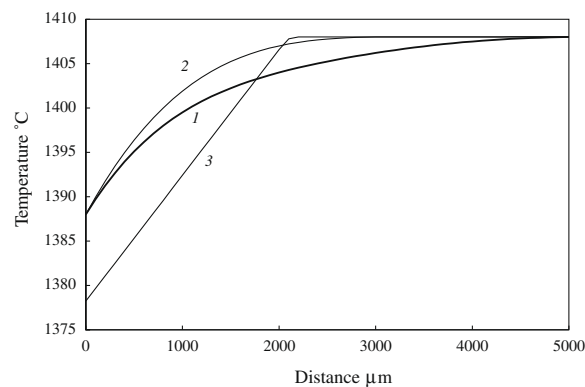


Fig. 12. Three temperature distributions used for calculating the thermal isotopic fractionations of iron shown in Fig. 11. The heavier curve labeled 1 corresponds to the temperature distribution shown in Fig. 1 based on the spinel thickness thermometry.

cause the diffusion of iron in the rhyolite is sufficiently slow that given the duration of the experiment the region affected is not much greater than 100 μm from the boundary. Note that the three choices for the temperature distribution do not significantly affect the calculated curves in the rhyolite side of the diffusion couple, which implies that the earlier estimate of $\beta = 0.030 \pm 0.005$ remains valid.

5. SUMMARY AND DISCUSSION

Table 1 lists the parameters that characterize experimentally measured kinetic isotope fractionations by chemical diffusion between molten basalt and rhyolite and by thermal diffusion in molten basalt. The fractionation of isotopes of a given element by chemical diffusion is parameterized in terms of the mass dependence of the diffusion coefficients by $D_i/D_j = (m_j/m_i)^\beta$. The value of the exponent β varies from 0.215 for Li ($D_{\text{Li}^{67}}$ is about 3.3% greater than $D_{\text{Li}^{7}}$) to 0.03 for Fe (such that $D_{\text{Fe}^{54}}$ is only 0.1% larger than $D_{\text{Fe}^{56}}$). A striking feature of our new results is that the isotopes of all the major elements of basalt can be very significantly fractionated by thermal diffusion as indicated by β_T being about an order of magnitude larger than the β for chemical diffusion. A further distinction between thermal and chemical isotope fractionations is that in the case of thermal diffusion the heavy isotopes of a given element have the larger thermal diffusion coefficients, which is opposite the mass dependence of the chemical diffusion coefficients. It is also worth noting that, at least for molten basalt, thermal diffusion always results in the heavy isotopes being enriched at the cold end regardless of whether the concentration of the parent element increases (i.e., Ca, Mg, Fe) or decreases (i.e., Si) towards the cold end.

Thermal isotope fractionations in silicate liquids have a variety of potentially important technological applications. The fact that we have shown that temperature differences of only 100 °C can produce nearly 1% fractionation of the entire inventory of ^{26}Mg and ^{24}Mg suggests that this approach could lead to effective methods for isotope separation, especially considering that much larger temperature differences could be used and that basalt is unlikely to

be the optimum liquid for such separations. Richter et al. (2008) pointed out that the thermal fractionation of magnesium isotopes provides a way of mapping the temperature distribution in a silicate melt that was held at high temperature in an experimental apparatus (i.e., a piston cylinder or multi-anvil press) for a sufficiently long time for the system to have reached a steady state and then rapidly quenched. The spatial distribution of the magnesium isotopes provides an excellent relative thermometer. $^{26}\text{Mg}/^{24}\text{Mg}$ can now be measured with a precision of about $\pm 0.1\%$ on 10–20 μm spots with a modern multi-collector ion microprobe (Kita et al., 2008), which when combined with the temperature sensitivity of the magnesium isotopes of about 4‰ per 100 °C per amu, indicates that temperature differences can be determined to about ± 2 °C. The fact that more than one isotopic system can now be used for such temperature mapping provides a way of validating the underlying assumption that the observed isotopic fractionations are a reliable proxy for temperature differences.

Richter et al. (2009) discussed a number of natural settings where kinetic isotopic fractionations by chemical diffusion appear to have played an important role. For example, the lithium diffused from a pegmatite into a surrounding amphibolite was shown by Teng et al. (2006) to be isotopically light by about 30‰ in a manner that is almost certainly due to ^6Li having diffused faster than ^7Li . Another example is the case of a silicate liquid evaporating into a low-pressure surrounding gas. Calcium–aluminum-rich inclusions (CAIs) in primitive meteorites are often enriched in the heavy isotopes of silicon and magnesium, which is generally believed to be the result of kinetic isotope fractionations during evaporation while molten (see review by Davis and Richter, 2007). The isotopic fractionation of evaporation residues has been documented by a variety of vacuum evaporation experiments (see for example Davis et al., 1990 for molten forsterite experiments, Richter et al., 2007 for molten CAI-like compositions). When applying the results of such experiments to material in the early protoplanetary disk that may have lost some fraction of the more volatile components by evaporation one has to allow for the possibility that evaporation might have been sufficiently fast that diffusion was not able to maintain an effectively homogeneous melt. The evaporation process would then be diffusion limited in that the surface concentration of the evaporating species would have to be replenished by diffusion from the interior. Our experiments show that this diffusion from the interior to the surface will also fractionate the isotopes, and this has to be taken into account when interpreting the isotopic composition of diffusion-limited evaporation residue. Richter (2004) discussed isotopic fractionation under diffusion-limited conditions, but at the time did not have experimental data of the sort reported here to quantify his arguments. Chondrules are another type of common inclusion in some meteorites (i.e., in chondritic meteorites that owe their name to these inclusions) and in many cases there is good evidence that they were also once molten droplets surrounded by a low pressure gas. However, in contrast to the CAIs, they are not significantly enriched in the heavy isotopes of their most volatile elements magnesium, iron and potassium de-

spite these elements being depleted to varying degrees relative to the more refractory elements. It has been suggested that the lack of isotopic fractionation of chondrules could be the result of extreme diffusion-limited evaporation (Galy et al., 2000; Young, 2000), but this would not explain the lack of isotopic fractionation because, as we have shown, the diffusive transport of magnesium and iron isotopes to the evaporating surface would still result in measurable isotopic fractionation of the residues. We expect the situation is similar for potassium, but do not yet have the relevant data regarding the isotopic fractionation of potassium by chemical diffusion in silicate melts.

Richter et al. (1999) have already discussed the possibility that a layered magma chamber might measurably fractionate isotopes as chemical elements diffused across double-diffusive interfaces between layers of different composition. The full range of thermodynamic and fluid dynamic processes that control the evolution of magma chambers are very diverse and complex. Here we will focus on more limited questions related to the isotopic fractionations that result due to chemical and thermal contrasts across a double-diffusive interface of the sort one expects in a magma chamber that is replenished by the intrusion of a chemically denser melt (Huppert and Sparks, 1980) or when a basaltic magma intrudes and melts the continental crust (Huppert and Sparks, 1988).

The model problem used here to explore the relative role of chemical gradients and thermal gradients in transporting elements and isotopes across a double-diffusive interface involves a deep, convectively well mixed, hot ($T = 1200$ °C) layer representing molten basalt under a layer of granitic melt initially at 800 °C. We focus on magnesium, and use a simplified version of Eq. (4) for the conservation equation for the mole fractions of ^{24}MgO , ^{25}MgO , ^{26}MgO , and total MgO. The simplification is to ignore the dependence of the chemical diffusion coefficient on the silica content of the melt, thus

$$\frac{\partial w_i}{\partial t} = D_i \frac{\partial}{\partial z} \left[\frac{\partial w_i}{\partial z} + \sigma_i w_i (1 - w_e) \frac{\partial T}{\partial z} \right] \quad (5)$$

where w_i can refer to the mole fraction ^{24}MgO , ^{25}MgO , ^{26}MgO , or the total MgO. w_e is the mole fraction of total MgO. The distance z is measured upwards (i.e., opposite the direction of gravity) from the interface. The mass dependence of the Soret coefficient $\sigma_i = D_T^i/D_i$ is parameterized using $\beta = 0.05$ and $\beta_T = 0.65$ (see Table 1). The energy equation written in terms of temperature is

$$\frac{\partial T}{\partial t} = \kappa \frac{\partial^2 T}{\partial z^2} \quad (6)$$

where κ is the thermal diffusivity. Eqs. (5) and (6) are used to model the transport of heat and chemical species into the granitic layer. The basalt layer is assumed to be sufficiently large and well-mixed by vigorous convection that it does not change significantly on the time scales considered and thus, to a first approximation, applies a constant temperature and composition boundary condition at the base of the granitic layer. The more complete problem would involve connecting the boundary layers in the basalt and granite by continuity of flux requirements, specifying the

thickness of the layers, and allowing for the temporal evolution of the bulk properties of the layers including effects such as crystallization. We will not address this more complete problem for the evolution of a layered intrusion because for the moment we want to focus on understanding the relative importance of chemical and thermal gradients in determining the chemical and isotopic fluxes across a double diffusive boundary. A key issue is whether the flux into the granitic layer will be isotopically light due to chemical diffusion or isotopically heavy when the thermally driven flux dominates the relative transport of the isotopes. Eqs. (5) and (6) are nondimensionalized to make more explicit the parameters that govern the double-diffusive fluxes and associated isotopic fractionations. We let $w_i = w_{i,g} + \Delta w_i w'_i$ where $\Delta w_i = w_{i,b} - w_{i,g}$, and $w_{i,g}$ and $w_{i,b}$ are the initial mole fractions of ^{24}MgO , ^{25}MgO , ^{26}MgO , or total MgO in the granite and basalt respectively. w'_i then is nondimensional going from one in the basalt to zero in the granite far from the interface. We let $T = T_g + \Delta T T'$ where, $\Delta T = T_b - T_g$, and T_g and T_b are the initial temperature of the granite and the basalt ($0 \leq T' \leq 1$). Distance is nondimensionalized by $z = L z'$ where L is chosen to be large compared to temperature and chemical boundary layers that develop at the interface. For time we let $t = (L^2/\kappa)t'$. When these relationships between the dimensional and primed nondimensional variables are substituted into Eqs. (5) and (6), they become after dropping primes,

$$\frac{\partial w_i}{\partial t} = \frac{\partial}{\partial z} \left\{ (D_i/\kappa) \left[\frac{\partial w_i}{\partial z} + \sigma_i \Delta T w_i \frac{\partial T'}{\partial z} \right] \right\} \quad (7)$$

and

$$\frac{\partial T}{\partial t} = \frac{\partial^2 T}{\partial z^2} \quad (8)$$

Eq. (7) includes a further simplification of replacing $1 - w_e$ with 1, which reduces the number of unknowns and is justified in that this term always close to one in the granite while w_i and T vary between 0 and 1. The initial conditions in terms of the nondimensional variables in the granitic layer are $w_i = 0$ and $T = 0$ at $t = 0$. The boundary conditions for the granitic layer are $w_i = 1$ and $T = 1$ at $z = 0$ and $w_i = 0$ and $T = 0$ at a sufficiently large value of z that changes would not be felt there. The nondimensional parameters that govern the initial diffusive evolution of the system are $\sigma_i \Delta T$ and D_i/κ . Assuming a temperature of 1200 °C for the basalt and 800 °C for the granite, $\Delta T = 400$ °C and using $\sigma_i = 0.0015$ for magnesium (Table 1), $\sigma_i \Delta T \sim 0.6$. A reasonable value for κ is 10^{-2} cm²/s (see Table 1 in Huppert and Sparks (1988) for a list of reasonable physical parameters for molten basalt and granite) and the chemical diffusion coefficient of magnesium in the granitic melt at the temperature of the interface will be in the range 10^{-6} – 10^{-10} cm²/s depending mainly on the amount of water dissolved in the melt (Watson, 1981). Thus D_{Mg}/κ will be a very small number in the range 10^{-4} – 10^{-8} . The model problem outlined above can be used to compare isotopic fractionations due only to chemical diffusion across the interface (i.e., by setting $\sigma_i \Delta T = 0$) with the results when thermal fractionations are allowed (i.e., when $\sigma_i \Delta T = 0.6$).

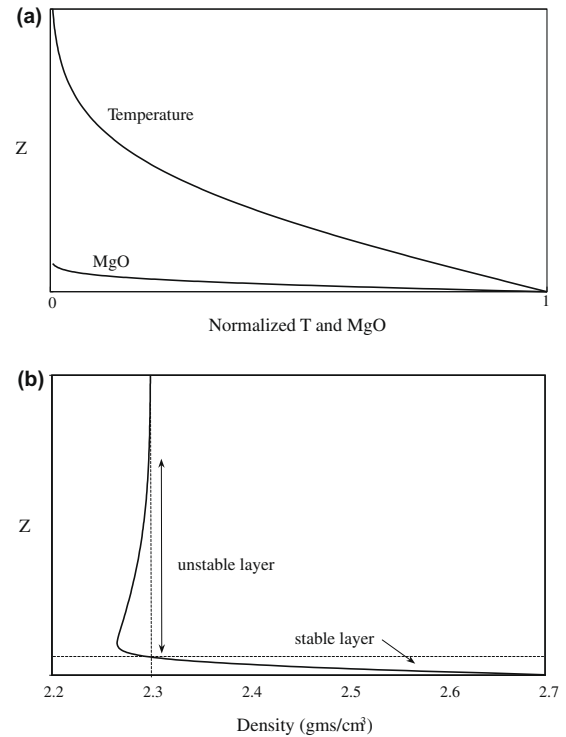


Fig. 13. (a) Vertical structure of the nondimensional temperature and mole fraction magnesium diffused into the granitic layer overlying molten basalt in the limit $\sigma_i \Delta T \rightarrow 0$. The vertical scale increases as a function of time as $t^{1/2}$. For purposes of illustration, the chemical boundary layer thickness was made especially large by assuming $D_{\text{Mg}}/\kappa = 10^{-4}$, which is at the high end of the range of realistic values for D_{Mg}/κ in molten granite. (b) The density as a function of distance above the basalt–granite interface showing the opposed effects of temperature and composition. Immediately above the interface a gravitationally stable layer develops due to the strong effect of composition changes on the density. Further from the boundary a hot, eventually unstable, layer develops due to the density there being lower than that of the overlying granitic melt.

The solution of Eq. (8) is $T = 1 - \text{erf}(z/\sqrt{4t})$. Solutions of Eq. (7) for the magnesium mole fractions when $\sigma_i \Delta T = 0$ and D_i/κ is independent of z is $w_i = 1 - \text{erf}(z/\sqrt{4(D_i/\kappa)t})$. In the limit $\sigma_i \Delta T \rightarrow 0$ the temperature and concentration solutions are same except for the length scale, which for concentration is smaller by a factor of 10^2 – 10^4 . Fig. 13 shows the structure of the two solutions along with the associated density profile. The density profile is calculated from the dependence of the density on temperature and composition as given by $\rho(T', w'_e) = \rho_{\text{granite}}(1 - \alpha \Delta T T' + \gamma w'_e)$ with $\rho_{\text{granite}} = 2.3$ g/cm³. We assume $\alpha = 5 \times 10^{-5}$ and $\gamma = 0.2$, which results in a reasonable density for the molten basalt of 2.7 g/cm³. In this formulation of the density the mole fraction of magnesium is used as a proxy for the bulk composition, which is justified in that all the major elements diffusing between basalt and rhyolite do so at very similar rate (see Fig. 3 in Richter et al., 2003).

Fig. 14 shows the calculated isotopic fractionation of magnesium in the chemical boundary layer shown in Fig. 13a, when only chemical diffusive transport is taken

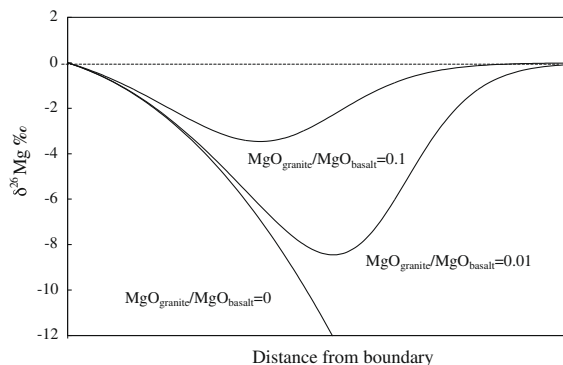


Fig. 14. Calculated magnesium isotopic fractionation as a function of distance in the chemical boundary layer shown in Fig. 13a. The three curves correspond to different choices for the initial relative amounts of magnesium in the basalt and granite. The lower the initial amount of magnesium in the granite the greater the isotopic fractionation because of less dilution of the transported magnesium by the original magnesium content of the granite. The isotopic fraction calculated for $\text{MgO}_{\text{granite}}/\text{MgO}_{\text{basalt}} = 0.01$ is very much like the observed isotopic fractionation of magnesium in sample SRT4 (see Fig. 5 in Richter et al., 2008). The bulk isotopic fractionation of the boundary layer is -2.0‰ , -1.9‰ , and -1.3‰ for the ratio of the magnesium concentration in the granite relative to that in basalt of 0, 0.01, and 0.1.

into account. The magnitude of the fractionation depends on the original amount of magnesium in the granite because the magnesium in the boundary layer is a mixture of the unfractionated original magnesium and the fractionated transported magnesium. The effect of including thermal diffusion of magnesium (i.e., setting $\sigma_i \Delta T = 0.6$ in Eq. (7)) on the concentration and isotopic fractionation in the boundary layer can be estimated by noting that in the limit $D_{\text{Mg}}/\kappa \ll 1$, the thermal gradient in the chemical boundary layer will be effectively dT/dz evaluated at $z=0$. For $T = 1 - \text{erf}(z/\sqrt{4t})$, $dT/dz|_{z=0} = -1/\sqrt{\pi t}$ while for magnesium $dw_e/dz|_{z=0} = -1/\sqrt{\pi(D_{\text{Mg}}/\kappa)t}$. The ratio of the thermally driven flux of magnesium to that due to chemical diffusion is independent of time and given by

$$\frac{J_{\text{Mg}}^{\text{thermal}}}{J_{\text{Mg}}^{\text{chemical}}} = \frac{\sigma_{\text{Mg}} \Delta T w_{\text{Mg}} (dt/dz)_{z=0}}{dw_{\text{Mg}}/dz} \approx \sqrt{D_{\text{Mg}}/\kappa} \ll 1 \quad (9)$$

Thus, the thermally driven flux of magnesium will have negligible effect on the results shown in Figs. 13 and 14, which we confirmed by how little the fractionations changed when the model was recalculated with $\sigma_i \Delta T = 0.6$.

Richter et al. (1999) calculated the chemical and isotopic evolution of a two-layer system assuming that the diffusive boundary layers shown in Figs. 13 would, once sufficiently thick, become convectively unstable, detach, and then be replaced by fluid with the bulk composition of the overlying layer. The relevant stability parameter for the boundary layer is the Rayleigh number, $Ra = \frac{g(\Delta\rho/\rho)d^3}{\kappa\nu}$ where g is the acceleration of gravity, $\Delta\rho/\rho$ is the fractional change in density in the boundary layer of thickness d , κ is the thermal diffusivity and ν is the kinematic viscosity. A boundary layer is expected to go unstable and detach once there is a sufficiently thick layer of low-density fluid such that the Rayleigh number based on this thickness exceeds a value

of about 2000. Heat transport calculated assuming the repeated breakdown of such an unstable boundary layer (Howard, 1964) has become a commonly used representation of transport due to vigorous thermal convection and a modified version of this was used by Linden and Shirtcliffe (1978) to interpret the transport of heat and salt in double diffusion experiments. If, as was assumed by Richter et al. (1999), the entire boundary layer is repeatedly stripped off, mixed into the interior and reformed, then the net time averaged dimensional fluxes \bar{J}_i are given by $\bar{J}_i = \frac{\rho \Delta w_i}{\tau} \int_0^\infty w_{i(z,\tau)} dz$ where τ is the recurrence time of stripping the boundary layer. The recurrence time can be estimated by the requirement that the boundary layer needs to have grown to the point where $Ra \sim 2000$. Huppert and Sparks (1988) estimated this time to be about 7 days for the detachment of the thermal boundary in a granitic melt (in their case for $T = 850^\circ\text{C}$ with 2% H_2O) above 1200°C basalt. At the time of detachment the thickness of the thermal boundary layer would be about 1 m. The chemical boundary layer would be thinner by an amount $\sqrt{D_{\text{Mg}}/\kappa}$, which will be 10^{-2} or less. For $\sqrt{D_{\text{Mg}}/\kappa} = 10^{-2}$, the chemical boundary layer will be about 1 cm thick at the time of instability and thus the magnesium flux will be about 0.1 mol magnesium per year per cm^2 and the isotopic composition of the transported magnesium will be light by about 1‰ per amu. The total amount and impact of this transported magnesium will depend on the initial temperature and magnesium concentration in the layers, the thickness of the layers and the duration of convection. Estimating these quantities in specific natural settings is beyond the scope of the present paper. The interested reader should refer to works by Huppert and Sparks (e.g., Huppert and Sparks, 1980, 1988) who discuss in detail the thermal evolution of convecting magma chambers of various sorts.

The assumption that the entire boundary layer at the interface between two actively convecting magma layers is repeatedly stripped away and mixed into the interior of the layers is reasonable for calculating the time averaged heat transport. However, it may not be a good assumption when it comes to chemical transports across the interface. Linden and Shirtcliffe (1978) developed a model for the double-diffusive interface to explain the results of laboratory experiments based on the assumption that the boundary layer is not stripped all the way to the interface but rather only to the level of neutral stability where the opposing effects of temperature and composition on the density cancel each other. In terms of density profile shown in Fig. 13b, only that part of the boundary layer that is less dense than the overlying fluid would be stripped away. Linden and Shirtcliffe (1978) showed that the stable layer in Fig. 13b would increase in thickness as long as the chemical flux into the layer was not balanced by removal of material into the overlying layer. Fig. 15 shows the result of our calculation for the development of such chemical diffusive core as a function of time from $t' = 0.1$ just before the first stripping away of the boundary layer to $t' = 50$, just before the boundary layer would have been stripped for the 500th time. In these calculations the boundary layer was stripped down to the level where $\alpha \Delta T t' = \gamma w'_e$. After $t' = 50$, the

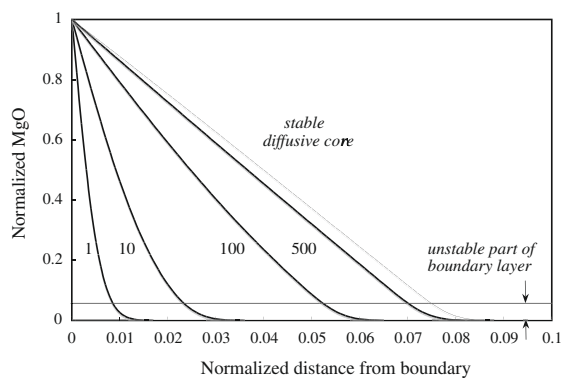


Fig. 15. Evolution of the diffusive core that develops at the base of the rhyolite layer when the convective detachment only strips the positively buoyant part of the boundary layer. The heavy solid curves show calculated MgO profiles at various times immediately before the unstable part of the boundary layer would have been stripped for the number of times indicated by the numbers by each curve. The chemical flux due to thermal diffusion was neglected (i.e., $\sigma\Delta T = 0$) except for the dashed curve that shows the effect of $\sigma\Delta T = 0.6$ on the thickness of the diffusive core just prior to the 500th removal of the unstable part of the chemical boundary layer. MgO is normalized by the value in basalt and distance is normalized by the thickness L of the thermal boundary layer that becomes unstable once $Ra = g(\Delta\rho/\rho)L^3/\kappa\nu = 2000$.

thickness of the diffusive core no longer increases to any significant degree because the chemical flux due to the linear gradient in the core is being balanced by the time-averaged flux due to the stripping of the small unstable part of the chemical boundary layer. Also shown in Fig. 15 is the small but no longer negligible effect of the thermally driven flux on the final thickness of the diffusive core. The diffusive core is still sufficiently thin that it has little effect on the temperature gradient and thus there is no significant change in the thermally driven chemical flux. The reason the thermally driven flux now has a measurable effect on the chemical profile is that it becomes a larger fraction of the total chemical transport as the chemical gradient in the diffusive core decreases with time.

While the impact of thermally driven flux is relatively minor in terms of the concentration of MgO, its effect on the isotopic fractionation is much more significant. Fig. 16 shows the isotopic fractionation of magnesium associated with the concentration profiles shown in Fig. 15. At early times when the magnesium flux is overwhelmingly due to the steep composition gradients, the isotopic fractionations are negative. However, as the diffusive core develops and the chemical gradient declines, the thermally driven flux of magnesium becomes proportionately more important. Eventually the isotopic fractionations become positive because the thermal flux is much more effective at fractionating the magnesium isotopes (i.e., $D_T^i/D_T^j = (m_i/m_j)^{0.65}$ while $D_i/D_j = (m_j/m_i)^{0.05}$) and does so in the direction of the heavy isotopes becoming enriched towards the colder parts. The small negative magnesium isotopic fractionations at the far edge of the diffusive core are due to chemical diffusion of magnesium into that part of the boundary layer that will be stripped away.

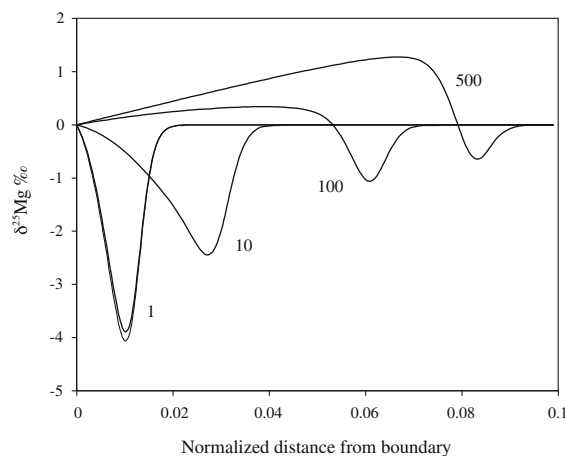


Fig. 16. The heavy curves show isotopic fractionations of magnesium in the chemical boundary layer and diffusive core at times corresponding to the MgO profiles shown in Fig. 15 calculated using $\sigma\Delta T = 0.6$ and $MgO_{\text{granite}}/MgO_{\text{basalt}} = 0.01$. The thin line at $t = 1$ was calculated neglecting the effect of temperature. It is very little different from the heavy curve at $t = 1$, which confirms that until a diffusive core develops the effect of the thermally driven chemical and isotopic fluxes have little effect compared to that of the fluxes driven by chemical gradients alone.

The purpose of these admittedly simplified model calculations for the thermal and chemical structure of a doubly-diffusive boundary layer in a convecting molten silicate system is to illustrate the competing effects of the thermally driven and chemically driven fluxes of a major component such as MgO. The key issue regarding the boundary layer structure is whether or not the entire boundary layer would be stripped off by repeated buoyancy driven convective instability, or if only the positively buoyant part would be removed. The model calculation by Richter et al. (1999) assumed that the entire boundary layer would be removed and that the repeated removal of the isotopically light material in the boundary layer might give rise to an observable net bulk fractionation between different levels of a layered intrusive system. The results of laboratory experiments of double-diffusive interfaces interpreted in the manner of Linden and Shirtcliffe (1978) lead us to believe that it is more likely that a stable diffusive core will develop at the interface between convecting melt layers. When this is the case, the thermally driven chemical fluxes could dominate the fractionation of the isotopes of all the major elements of silicate melt transported across the interface. However, these fractionations will for the most part be restricted to the diffusive core and we now suggest that the best place to look for isotopic evidence of double diffusive exchange in molten silicate system might not be in the interior of the layers, but rather in a thin diffusive core at the interface.

In closing we should reemphasize the point made in Figs. 5, 7 and 11 that even small temperature differences of a few tens of degrees, if sustained for a sufficiently long time, will result in large (relative to analytical precision) fractionations of the isotopes of all the major elements except aluminum of a silicate liquid such as basalt. Furthermore, as we showed in Fig. 6, such thermal isotopic fractionations will be correlated in predictable ways, which

provides a powerful diagnostic for distinguishing thermal isotope fractionations from those arising from other natural or un-natural processes.

ACKNOWLEDGMENTS

This work was supported by DOE Grant (DE-FG02-01ER15254,A005) and NASA Grant (NNG06GE85G) to Frank Richter, NSF Grant EAR-0337481 to Bruce Watson, by a fellowship from the Packard Foundation, the France Chicago Center, and NASA Grant NNG06GG75G to Nicolas Dauphas, and DOE Grant FG02-93ER14389 to John Valley. Jim Watkins was supported by LLNL IGPP Award #07-GS-008. The Si isotopic analyses by Bastian Georg were made possible by funding from PPARC and Oxford University. We also thank Mike Spicuzza of the Department of Geology and Geophysics at UW-Madison for the oxygen isotope analyses.

REFERENCES

- Dauphas N., Janney P. E., Mendybaev R. A., Wadhwa M., Richter F. M., Davis A. M., van Zuilen A., Hines R. and Foley C. N. (2004) Chromatographic separation and multicollection-ICPMS analysis of iron. Investigating mass-dependent and independent isotope effects. *Anal. Chem.* **76**, 5855–5863.
- Dauphas N. and Rouxel O. (2006) Mass spectrometry and natural variations of iron isotopes. *Mass Spectrom. Rev.* **25**, 515–550.
- Dauphas N., Pourmand A. and Teng F.-Z. (in press) Routine isotopic analysis of iron by HR-MC-ICPMS: how precise and how accurate? *Chem. Geol.*
- Davis A. M., Hashimoto A., Clayton R. N. and Mayeda T. K. (1990) Isotope mass fractionation during evaporation of forsterite (Mg₂SiO₄). *Nature* **347**, 655–658.
- Davis A.M. and Richter F.M. (2007) Condensation and evaporation of solar system materials – revised. In *Meteorites, Comets, and Planets* (ed. A.M. Davis) Vol. 1 *Treatise on Geochemistry*, 1 (eds., H. D. Holland and K. K. Turekian). Elsevier-Pergamon, Oxford.
- deGroot S. R. and Mazur P. (1984) *Non-Equilibrium Thermodynamics*. Dover Publications, New York, 510 pp.
- DePaolo D. J. (2004) Calcium isotopic variations produced by biological, kinetic, radiogenic and nucleosynthetic processes. *Rev. Mineral. Geochem.* **55**, 255–288.
- Fantle M.S. (2005) The global geochemical cycles of iron and calcium: using novel isotope systems to understand weathering, global mass budgets, natural reaction rates, and paleoclimate. Ph. D. dissertation, University of California-Berkeley.
- Galy A., Young E. D., Ash R. D. and O’Nions R. K. (2000) The formation of chondrules at high gas pressures in the solar nebula. *Science* **290**, 1751–1753.
- Georg R. B., Reynolds B. C., Frank M. and Halliday A. N. (2006) New sample preparation techniques for the precise determination of the Si isotope composition of natural samples using MC-ICP-MS. *Chem. Geol.* **235**, 95–104.
- Howard L.N. (1964) Convection at High Rayleigh Number. *Proc. 11th Int. Cong. Appl. Mech.*, Springer, pp. 1109–1115.
- Huppert H. E. and Sparks R. S. J. (1980) The fluid dynamics of a basaltic magma chamber replenished by influx of hot, dense ultrabasic magma. *Contrib. Mineral. Petrol.* **75**, 279–289.
- Huppert H. E. and Sparks R. S. J. (1988) The generation of granitic magmas by intrusion of basalt into continental crust. *J. Petrol.* **29**, 599–624.
- Kita N. T., Ushikubo T., Fournelle J., Knight K. B., Mendybaev R. A., Davis R. A. and Richter F. M. (2008) Internal isochron of CAI using high precision SIMS Mg isotope analyses. *Geochim. Cosmochim. Acta* **72**, A447 (abstr.).
- Kyser T. K., Leshner C. E. and Walker D. (1998) The effects of liquid immiscibility and thermal diffusion on oxygen isotopes in silicate liquids. *Contrib. Mineral. Petrol.* **133**, 373–381.
- Leshner C. E. and Walker D. (1986) Solution properties of silicate liquids from thermal diffusion experiments. *Geochim. Cosmochim. Acta* **50**, 1397–1411.
- Linden P. F. and Shirtcliffe T. G. L. (1978) The diffusive interface in double-diffusive convection. *J. Fluid Mech.* **87**, 417–432.
- Richter F. M., Liang Y. and Davis A. M. (1999) Isotope fractionation by diffusion in molten oxides. *Geochim. Cosmochim. Acta* **63**, 2853–2861.
- Richter F. M., Davis A. M., DePaolo D. J. and Watson E. B. (2003) Isotope fractionation by chemical diffusion between molten basalt and rhyolite. *Geochim. Cosmochim. Acta* **67**, 3905–3923.
- Richter F. M. (2004) Timescales determining the degree of kinetic isotope fractionation by evaporation and condensation. *Geochim. Cosmochim. Acta* **68**, 4971–4992.
- Richter F. M., Watson E. B., Mendybaev R. A., Teng F.-Z. and Janney P. E. (2008) Magnesium isotope fractionation in silicate melts by chemical and thermal diffusion. *Geochim. Cosmochim. Acta* **72**, 206–220.
- Richter F. M., Dauphas N. and Teng F.-Z. (2009) Non-traditional fractionation of non-traditional isotopes by chemical and Soret diffusion. *Chem. Geol.* **258**, 92–103.
- Richter F. M., Janney P. E., Mendybaev R. A., Davis A. M. and Wadhwa M. (2007) Elemental and isotopic fractionation of Type B CAI-like liquids by evaporation. *Geochim. Cosmochim. Acta* **71**, 5544–5564.
- Skulan J., DePaolo D. and Owens T. (1997) Biological control of calcium isotopic abundances in the global calcium cycle. *Geochim. Cosmochim. Acta* **61**, 2505–2510.
- Teng F.-Z., McDonough W. F., Rudnick R. L. and Walker R. J. (2006) Diffusion-driven extreme lithium isotopic fractionation in country rocks of the Tin Mountain pegmatite. *Earth Planet. Sci. Lett.* **243**, 701–710.
- Tyrell H. J. V. (1961) *Diffusion and Heat in Liquids*. Butterworths, London, pp. 329.
- Valley J. W., Kitchen N. E., Kohn M. J., Niendorf C. R. and Spicuzza M. J. (1995) UWG-2, A garnet standard for oxygen isotope ratio: strategies for high precision and accuracy with laser heating. *Geochim. Cosmochim. Acta* **59**, 5223–5231.
- Watson E. B. (1981) Diffusion in magmas at depth in the Earth: The effects of pressure and dissolved H₂O. *Earth Planet. Sci. Lett.* **52**, 291–301.
- Watson E. B., Wark D. A., Price J. D. and Van Orman J. A. (2002) Mapping the thermal structure of solid-media pressure assemblies. *Contrib. Mineral. Petrol.* **142**, 640–652.
- Young E. D. (2000) Assessing the implications of K isotope geochemistry in the planetary nebula. *Earth Planet. Sci. Lett.* **183**, 321–333.

Associate editor: F.J. Ryerson